International Journal of Nanomedicine

Dovepress
open access to scientific and medical research

Open Access Full Text Article

ORIGINAL RESEARCH

Graphene Oxide-Template Gold Nanosheets as Highly Efficient Near-Infrared Hyperthermia Agents for Cancer Therapy

This article was published in the following Dove Press journal:
International Journal of Nanomedicine

Shuyi He[1–3,*]
Jingyu Li[1–3,*]
Mingjian Chen[1–3]
Liehua Deng[4]
Yuxin Yang[1–3]
Zhaoyang Zeng[1–3]
Wei Xiong[1–3]
Xu Wu[1–3]

[1]NHC Key Laboratory of Carcinogenesis and Key Laboratory of Carcinogenesis and Cancer Invasion of the Chinese Ministry of Education, Cancer Research Institute and School of Basic Medical Science, Central South University, Changsha, People's Republic of China; [2]Hunan Key Laboratory of Nonresolving Inflammation and Cancer, Disease Genome Research Center, The Third Xiangya Hospital, Central South University, Changsha, People's Republic of China; [3]Hunan Key Laboratory of Translational Radiation Oncology, Hunan Cancer Hospital and the Affiliated Cancer Hospital of Xiangya School of Medicine, Central South University, Changsha, People's Republic of China; [4]Department of Critical Care Medicine, Affiliated Hospital of Guangdong Medical University, Zhanjiang, People's Republic of China

*These authors contributed equally to this work

Correspondence: Xu Wu
Central South University, 110 Xiangya Road, Kaifu District, Changsha City, Hunan Province 410078, People's Republic of China
Email wuxu1028@csu.edu.cn

Introduction: Near-infrared (NIR) hyperthermia agents are promising in cancer photothermal therapy due to their deeper penetration ability and less side effects. Spherical gold nanoshell and graphene-based nanomaterials are two major NIR hyperthermia agents that have been reported for photothermal therapy of cancer. Herein, we constructed a two-dimensional graphene oxide-template gold nanosheet (GO@SiO_2@AuNS) hybrid that could destruct cancer cells with efficient photothermal effect.

Methods: Graphene oxide was coated with a layer of mesoporous silica, which provided binding sites for gold seeds. Then, seed-growth method was utilized to grow a layer of gold nanosheet to form the GO@SiO_2@AuNS hybrid, which possessed great biocompatibility and high photothermal conversion efficiency.

Results: With the irradiation of NIR laser (808 nm) with low power density (0.3 W/cm^2), GO@SiO_2@AuNS hybrid showed a photothermal conversion efficiency of 30%, leading to a temperature increase of 16.4 °C in water. Colorectal cancer cells (KM12C) were killed with the treatment of GO@SiO_2@AuNS hybrid under NIR irradiation.

Conclusion: The GO@SiO_2@AuNS hybrid may expand the library of the 2D nanostructures based on gold for cancer photothermal therapy.

Keywords: graphene oxide, gold nanosheets, photothermal therapy, near-infrared

Introduction

In the last few decades, cancer has become one of the leading causes of death in noncommunicable diseases for global population.[1] It is urgent to find effective treatments for cancer. The latest report released by the American Cancer Society in 2020 recognizes the value of new systemic cancer therapy in reducing the number of surgeries and even reducing the need for surgery. Considerable progress has been made in the systematic treatment of pancreatic cancer, renal cancer, prostate cancer, and melanoma, which have reshaped surgical treatment, making it one of the most impressive achievements this year.[2] Compared with traditional therapies, including surgery, chemotherapy and radiotherapy, new therapeutic strategies, such as immunotherapy, gene therapy, photodynamic therapy and photothermal therapy can overcome the shortcomings of the traditional therapies,[3–5] including sever side-effect, multidrug resistance (MDR) and radiotherapeutic resistance.[6] Photothermal therapy (PTT) is a noninvasive therapeutic mode to kill cancer cells with hyperthermia using laser irradiation. Photothermal agents absorb

laser irradiation and release thermal energy to enhance the temperature of the microenvironment of cancer (thermal ablation, with temperature higher than 45 °C), which results in cancer cell death. On the other hand, PTT can also induce mild-temperature increase (with temperature of 40 ~ 45 °C) in tumor tissues to increase the sensitivity of cancer cells for other treatments such as chemotherapy and radiotherapy, which ultimately achieves a synergistic treatment effect.[7,8]

A lot of photothermal agents have been introduced for cancer photoablation, such as cyanine-based NIR dyes,[9–11] polypyrrole nanoparticles (NPs),[12] polyaniline NPs,[13] and metal NPs.[14] Among them, gold nanomaterials with different structures are promising because of their excellent photothermal conversion capability[15] and facile surface modification with other ligands for specific tumor targeting.[16–18] In addition, due to the inherent biological inertness, high surface area ratio, and tunable large absorption cross-section in the near-infrared region (NIR), gold nanomaterials are ideal photothermal agents for cancer therapy.[19,20] Although a number of gold nanomaterials, including gold nanoparticles,[21] gold nanorods,[22] gold nanostars,[23] gold nanoshell,[24] etc., have been developed in recent years for photothermal ablation of cancer, a few two-dimensional (2D) NIR gold nanosheets have been reported as photothermal agents. Tang et al recently prepared the 2D core-shell Mxene@gold nanocomposite by using Ti_3C_2 as a template.[25] But the long-term biosafety of MXenes remained a high-risk factor. Ideally, silica layer with high biocompatibility and stability was promising for fabricating zero-dimensional gold nanoshells for photothermal therapy, during which the silica layer was used as a template for anchoring gold seeds and gold shell growth. Taking the advantage of silica layer's properties, we are inspired to expand the library of 2D gold nanosheets to promote the development of highly efficient photothermal agents for cancer therapy.

Graphene oxide (GO) has unique physical, chemical, and mechanical characteristics, making it an ideal candidate for new biological applications. These properties include: (i) GO has a variety of oxygen-containing functional groups on its edges and basal planes, such as carbonyl, hydroxyl, carboxyl, and epoxy, for good water solubility and easy surface modification;[26] (ii) GO is mainly composed of carbon atoms which give them excellent biocompatibility and non-toxicity nature;[27] (iii) the large delocalized π-electron system helps GO to achieve an excellent adsorption capacity in the visible and near-infrared regions.[28] Due to these excellent properties of GO, it has been widely used for biomedical application as a 2D nanomaterial. For example, Gao et al designed an activatable GO/Au nanocomposite for photoacoustic and fluorescence imaging guided photothermal therapy of cancer.[29] Zeng et al used GO as a carrier to transport doxorubicin (DOX) and siRNA to drug-resistant tumor cells and enhanced the killing effect of DOX on tumor cells through the photothermal effect and gene silencing.[30] Recently, Liu et al prepared a reduced graphene oxide/mesoporous silica nanocomposite to combine pH-responsive chemotherapy and photothermal therapy for cancer treatment.[31] Based on these points, we believe the photothermal conversion efficiency could be significantly enhanced by coupling with 2D gold nanosheet on the template of GO.

In this work, a core-shell 2D gold nanosheet (GO@SiO_2@AuNS hybrid) was designed and prepared by a seed-growth approach for photothermal therapy of cancer using GO as a template (Scheme 1). The proposed GO@SiO_2@AuNS hybrid has several advantages. First, the 2D structure and mesoporous silica layer on GO not only provided the template for anchoring gold seeds and gold shell growth, but also increased the biocompatibility and stability of the GO. Second, the GO@SiO_2@AuNS hybrid showed strong absorption in the near-infrared region and photothermal conversion efficiency, which could kill cancer cells under mild NIR laser irradiation (0.3 W/cm^2). We comprehensively studied the photothermal therapeutic effect of the GO@SiO_2@AuNS hybrid in colorectal cancer cells (KM12C). Our results suggested that this novel 2D core-shell gold hybrid might provide potential applications in cancer treatment.

Methods and Materials

Materials and Instruments

Tetraethylorthosilicate (TEOS, 98%) was purchased from Acros Organics (Fisher Scientific, Fairlang, New Jersey, USA). Graphene oxide (~1.0 μm) was purchased from Cheap Tubes Inc. (Grafton, Vermont, USA). Gold (III) chloride trihydrate ($HAuCl_4 \cdot 3H_2O$, 99.9+%), hexadecyltrimethylammonium bromide (CTAB, CH3(CH2)15N(Br)-(CH3)3, 96%), hydroxylamine hydrochloride (98%, ACS grade), and sodium borohydride ($NaBH_4$, >98%) were purchased from Sigma Aldrich Inc (Milwaukee, Wisconsin, USA). Ammonium hydroxide (NH_4OH, 28.0–30.0%), potassium carbonate ($K_2CO_3 \cdot 1.5\ H_2O$, ACS grade), ethanol (95%), phosphate buffered saline tablets and fetal bovine serum

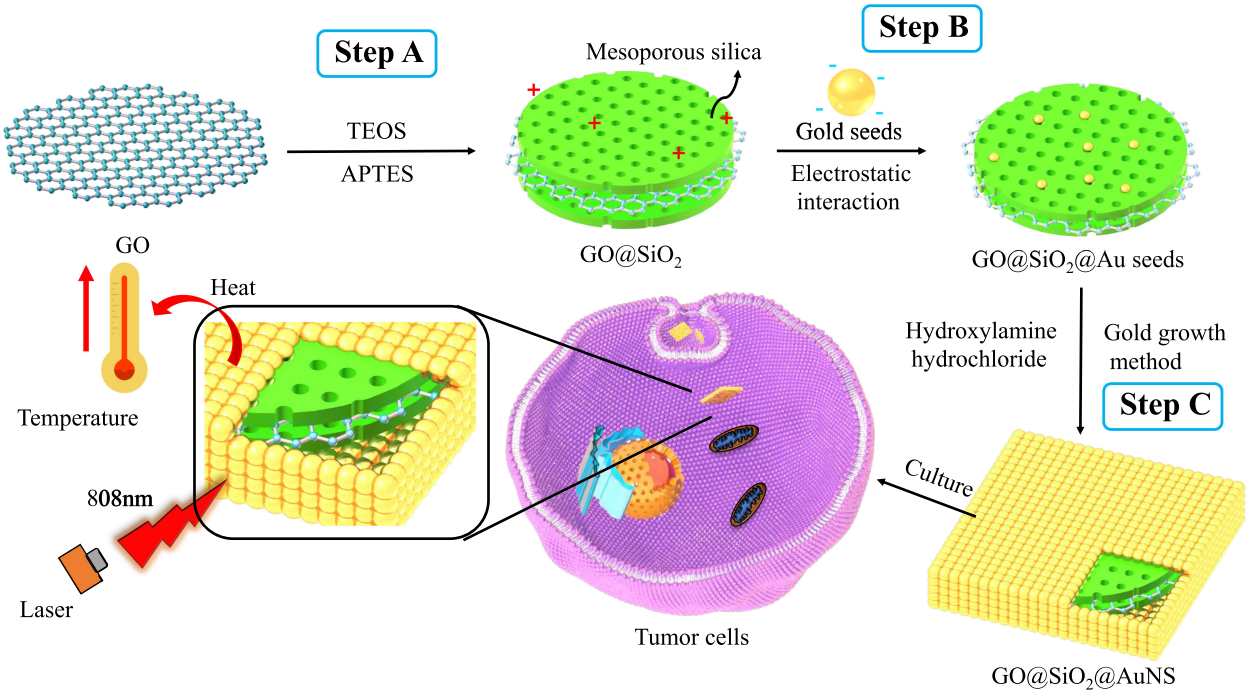

Scheme 1 Schematic illustration of the GO@SiO_2@AuNS hybrid formation for photothermal therapy of cancer cells.

were obtained from Fisher Scientific Co (Beijing, China). Polyvinylpyrrolidone molecule (PVP, average molecular weight Mn = 10,000) was purchased from Alfa Aesar (Shanghai, China). Human colon cancer cell line, KM12C and SW620 were obtained from Shanghai cell bank of Chinese Academy of Sciences. Deionized (DI) water (Millipore Milli-Q grade) with the resistivity of 18.2 MΩ•cm was used in all experiments (Millipore Sigma, Burlington, Massachusetts, USA).

A Hitachi SU8010 field emission scanning electron microscope (Hitachi, Tokyo, Japan) was used to take the SEM and STEM images of the RGO/Ag nanocomposite. Elemental analysis for different RGO/metal nanocomposites was performed by an energy-dispersive X-ray spectroscope (EDS) (Oxford, X-Max) installed in the Hitachi SU8010 SEM (Hitachi, Tokyo, Japan). UV-vis absorption spectra were recorded with a Perkin Elmer UV-Vis spectrometer (PerkinElmer, Waltham, Massachusetts, USA). The photothermal effect study was performed by a BWF1 series fiber-coupled diode laser system (808 nm) (B&W TEK Inc, Newark, Delaware, USA).

Synthesis of GO@SiO_2

The preparation of GO@SiO_2 was carried out according to a previous literature.[31] Briefly, 50 mL of 0.1 mg/mL GO aqueous solution was mixed with 500 mg CTAB and 20 mg sodium hydroxide under ultrasonication. Then, 250 µL TEOS was injected into the solution and stirred in a 40 °C water bath for 2 hours, followed by the addition of 50 µL APTES and stirred for another 5 hours. Finally, the formed GO@SiO_2 was centrifuged and refluxed in 50 mL HCl/EtOH solution (0.1%, v/v) for 3 hours to remove the surfactant and reactants. After washing with ethanol and water, the final product was re-dispersed in water with concentration of 10.0 mg/mL for further usage.

Preparation of Gold Seeds

Gold seeds were synthesized according to previous studies.[32] Firstly, 100.0 mL 0.04% $HAuCl_4$ was mixed with 0.5 mL 0.2 M K_2CO_3 in an ice bath with stirring, turning the bright yellow solution into colorless solution. Then, 5.00 mL of freshly prepared 0.5 mg/mL $NaBH_4$ solution was dropwise added to the solution with vigorous stir. The color of the solution became reddish, suggesting the formation of gold seeds, which was preserved at 4.0 °C for future usage.

Formation of GO@SiO_2@AuNS Hybrid

First, 1.0 mL of 10.0 mg/mL GO@SiO_2 solution was mixed with 40 mL of gold seeds solution, and vigorously stirred for 10 minutes to absorb Au seeds onto GO@SiO_2.

The solution was centrifuged at the speed of 6500 rpm for 10 min and the supernatant was abandoned to remove the excess gold seeds. The red sediment represented that the GO@SiO_2 was successfully coated with Au seeds, which was suspended in 10 mL water to obtain GO@SiO_2@Au seeds solution. The 10 mL of GO@SiO_2@Au seeds solution was added to the gold growth solution, which was composed of 2.00 mL (or 0.50, 1.00, or 4.00 mL) of 1.00% $HAuCl_4$ and 0.025g of K_2CO_3 in 90.00 mL of water. After stirring for 5 min, 1.00 mL of 0.50 M hydroxylamine hydrochloride was slowly injected into the above solution. Finally, 1.00 g of PVP as a stabilizer was added into the solution with overnight stirring. The GO@SiO_2@AuNS hybrid was obtained after the centrifugation at 6500 rpm for 15 min to remove the excess PVP and the final product was re-dispersed in water for further usage.

Cytotoxicity Investigation

The cytotoxicity of GO@SiO_2@AuNS hybrid was investigated in different cancer cells including KM12C and SW620 cells by MTT assay. Cells were seeded in 96-well plates at 37 °C for 24 hours, followed by the incubation with GO@SiO_2@AuNS hybrid with different concentrations (0, 10, 20, 40, 60, 80, 100 and 150 μg/mL) for 24 hours. Then, 10.00 μL MTT reagent was added into each well to reach a final concentration of 1.00 μg/mL. The cells were cultured at 37 °C for 4 h until purple-colored crystals appeared. Subsequently, each well was added 100.00 μL of stop solution (50 mM HEPES buffer of 10% SDS, 10% DMSO) and shaked for a while. An enzyme linked immunosorbent assay reader was employed to measure the absorbance of each well.

Photothermal Therapy in vitro

The effect of photothermal therapy was first evaluated using the above-mentioned MTT method. KM12C cells were seeded in 96-well plates at 37 °C for 24 h. Different concentrations of GO@SiO_2@AuNS (10, 50, and 100 μg/mL) or PBS solution (control) were incubated with KM12C cells for 6 h and then subjected to NIR irradiation for 0 min or 20 min using an 808 nm laser with power density of 0.3 W/cm^2. The cell viability was evaluated by MTT assay according to the above protocol.[33]

The Vybrant apoptosis assay was used to test cell apoptosis and necrosis. The GO@SiO_2@AuNS hybrid with different concentrations (0, 10, 50, and 100 μg/mL) in DMEM culture medium was incubated with KM12C cells overnight with the final cell number of ~1 × 10^5/well before the treatment. Then, the cells were irradiated with an 808 nm laser with power density of 0.3 W/cm^2 for 20 min. After being washed twice with fresh cell culture medium, the cells were stained with YO-PRO-1 dyes (Vybrant apoptosis assay kit) and propidium iodide (PI) for 10 min, followed by observation using a Zeiss confocal fluorescence microscope. The green fluorescence of YO-PRO-1 was excited with an Argon laser and collected with a 505–550 nm band-pass filter. The red fluorescence of PI was excited with Helium-Neon laser and collected with a 580 nm long-pass filter.

Results and Discussion

Synthesis and Characterization of GO@SiO_2@AuNS Hybrid

The synthesis of GO@SiO_2@AuNS hybrid is illustrated in Scheme 1 by three steps. First, the commercial GO was coated with a mesoporous silica layer through the sol-gel method using CTAB as a stabilizer and template (Scheme 1, step A). During the hydrolysis of saline (TEOS), amino-terminated saline (APTES) was co-hydrolyzed to modify amino groups on the surface of the mesoporous silica layer, which was used to anchor gold seeds. The SEM images of GO and GO@SiO_2 show that the wrinkle and smooth morphology, respectively (Figure 1A and B). However, the lateral size dramatically decreased from 1.0 μm to about 300 nm. This might be caused by the strong base and acid treatment during the synthesis process. But detail mechanism needs further investigation, which is not in the scope of this work. The hydrodynamic diameter measured by DLS showed a similar size of 300 nm of GO@SiO_2 (Figure 2A). The presence of the amino groups on the mesoporous silica layer could be evidenced by the positive surface potential (+10 mV) (Figure 2B).

In the second step, the prepared small gold seeds (~4 nm) were anchored to the positive-charged surface of GO@SiO_2 through electrostatic interaction (Scheme 1, Step B). After being removed the excess gold seeds, the GO@SiO_2@Au seeds clearly showed the decorated individual gold seed in SEM image (Figure 1C) and negative charges (−20 mV) (Figure 2B). In contrast, the lateral size and hydrodynamic diameter of GO@SiO_2@Au seeds did not change (Figure 1C and Figure 2A). The gold seeds on the silica layer provided anchoring sites for the growth of gold nanosheets in the following step.

In the last step, we utilized the gold growth method to prepare the 2D gold nanosheets on the surface of GO@SiO_2

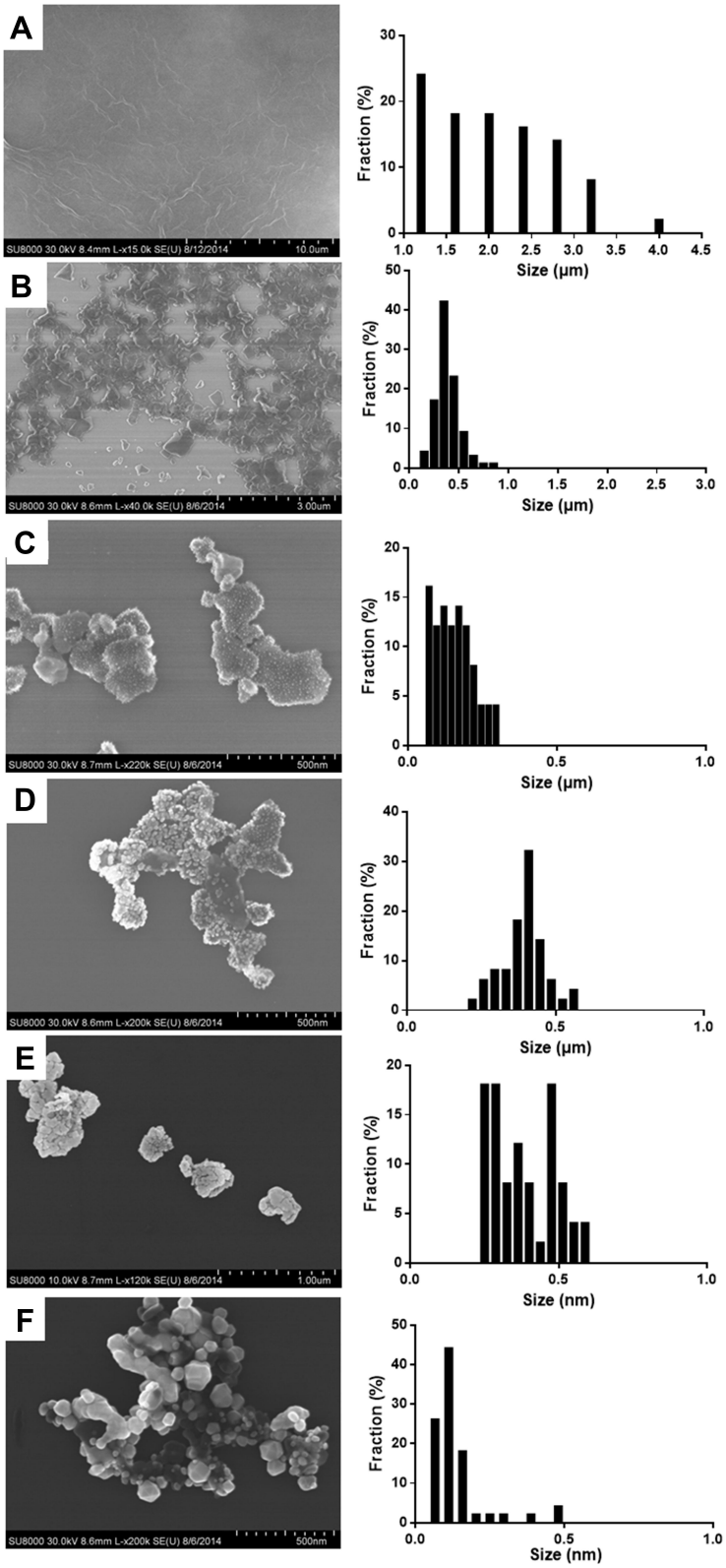

Figure 1 SEM images and size distribution of GO (**A**), GO@SiO_2 (**B**), GO@SiO_2@Au seeds (**C**) and GO@SiO_2@AuNS with different amount of 1 mL (**D**), 2mL (**E**) and 4 mL (**F**) of $HAuCl_4$. The right panels are the size distributions of these nanomaterials by measuring at least 100 nanomaterials.

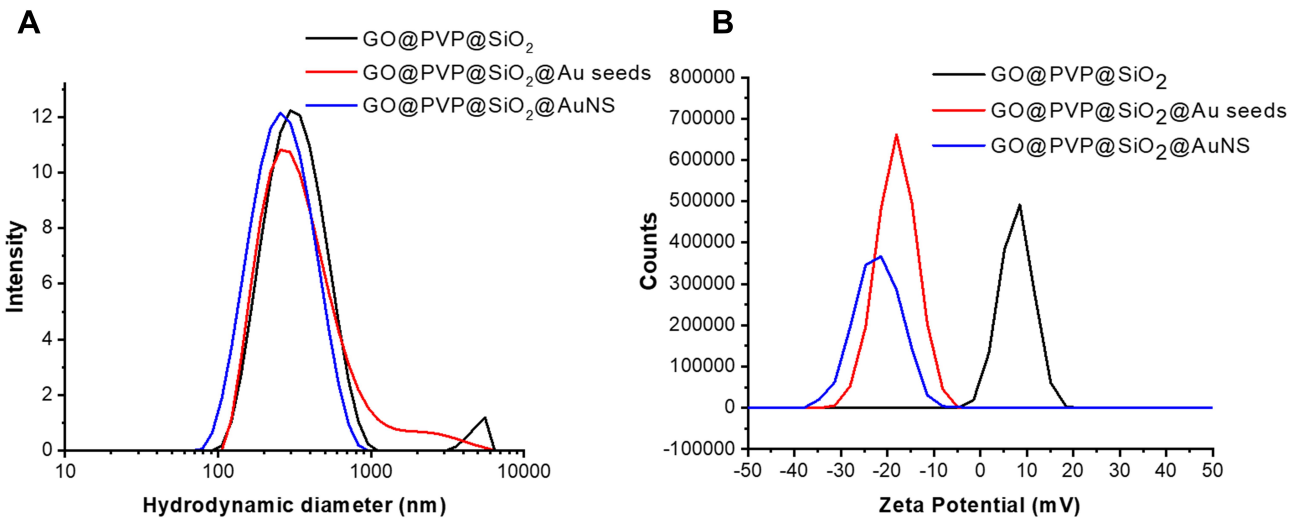

Figure 2 Hydrodynamic diameters (**A**) and zeta potential (**B**) of the synthesized nanomaterials.

@Au seeds (Scheme 1, Step C). A layer of gold sheet was formed on the outside of GO@SiO_2@Au seeds by introducing hydroxylamine hydrochloride to reduce $HAuCl_4$, followed by the modification of PVP through electrostatic interaction. The final product was designated as GO@SiO_2@AuNS hybrid. SEM images demonstrated the formation of the Au shell and the 2D structure of the hybrid (Figure 1D–F). The hydrodynamic diameters and surface zeta potentials of GO@SiO_2@AuNS hybrid have neglectable change compared with the GO@SiO_2@Au seeds. Furthermore, SEM images (Figure 1D–F) showed that the density of the Au shell was directly related to the amount of added $HAuCl_4$. The coverage of Au shell increased when the amount of the 1% $HAuCl_4$ increased from 1 mL to 4 mL in the gold growth solution. However, when 4 mL 1% $HAuCl_4$ was used for the synthesis of GO@SiO_2@AuNS hybrid, we noticed that more isolated free gold nanoparticles were formed, which was proved by the decreased size (right panel of Figure 1F).

To confirm the formation of the GO@SiO_2@AuNS hybrid, SEM-EDS elemental analysis was performed. As shown in Figure 3, the elemental mapping image and spectrum confirmed the presence of the Au, Si, O, and C in the GO@SiO_2@AuNS hybrid as designed, indicating the presence of GO, silica layer and gold shell, respectively. The Cu signal came from the copper grids used for holding the sample.

During the preparation of GO@SiO_2@AuNS hybrid, we characterized each step with absorption spectroscopy. The results demonstrated that the plasmon resonance band changed with the addition of the gold growth solution. As shown in Figure 4, the pure GO@SiO_2 revealed a low absorbance in the near-infrared region. With the addition of gold seeds on the surface of GO@SiO_2, an absorption peak at 520 nm was presented, indicating the successful adhesion of gold seeds on the surface of GO@SiO_2. During the gold growth process, the absorption of GO@SiO_2@AuNS hybrid could be easily tuned by adding different amounts of gold growth solution. When the amount of 1% $HAuCl_4$ in gold growth solution increased from 1 mL to 2 mL, the absorption peak of GO@SiO_2@AuNS hybrid showed a broad red-shift peak towards NIR (Figure 4). Compared with the GO@SiO_2, the GO@SiO_2@AuNS-2mL hybrid showed almost 40-times enhancement of the absorbance at 808 nm. This result indicated that GO@SiO_2@AuNS hybrid would be promising for photothermal therapy with NIR laser irradiation. However, when the amount of gold growth solution increased to 4 mL, the absorption peak at 520 nm was again presented coupled with decreased NIR absorbance, which suggested the formation of many free gold nanoparticles in the solution. Therefore, we chose the 2 mL of 1% $HAuCl_4$ in gold growth solution for the following experiments to prepare the optimal GO@SiO_2@AuNS hybrid for photothermal therapy.

Concentration Effect of GO@SiO_2@AuNS Hybrid on NIR Absorbance

Given that the plasmon resonance absorption intensity of nanomaterials is closely related to their concentration, we further evaluated the optical absorbance of GO@SiO_2@AuNS hybrid with various concentrations. The results showed a concentration dependent NIR absorbance for the GO@SiO_2@AuNS hybrid (Figure 5A). The absorbance of the GO@SiO_2@AuNS hybrid increased when its

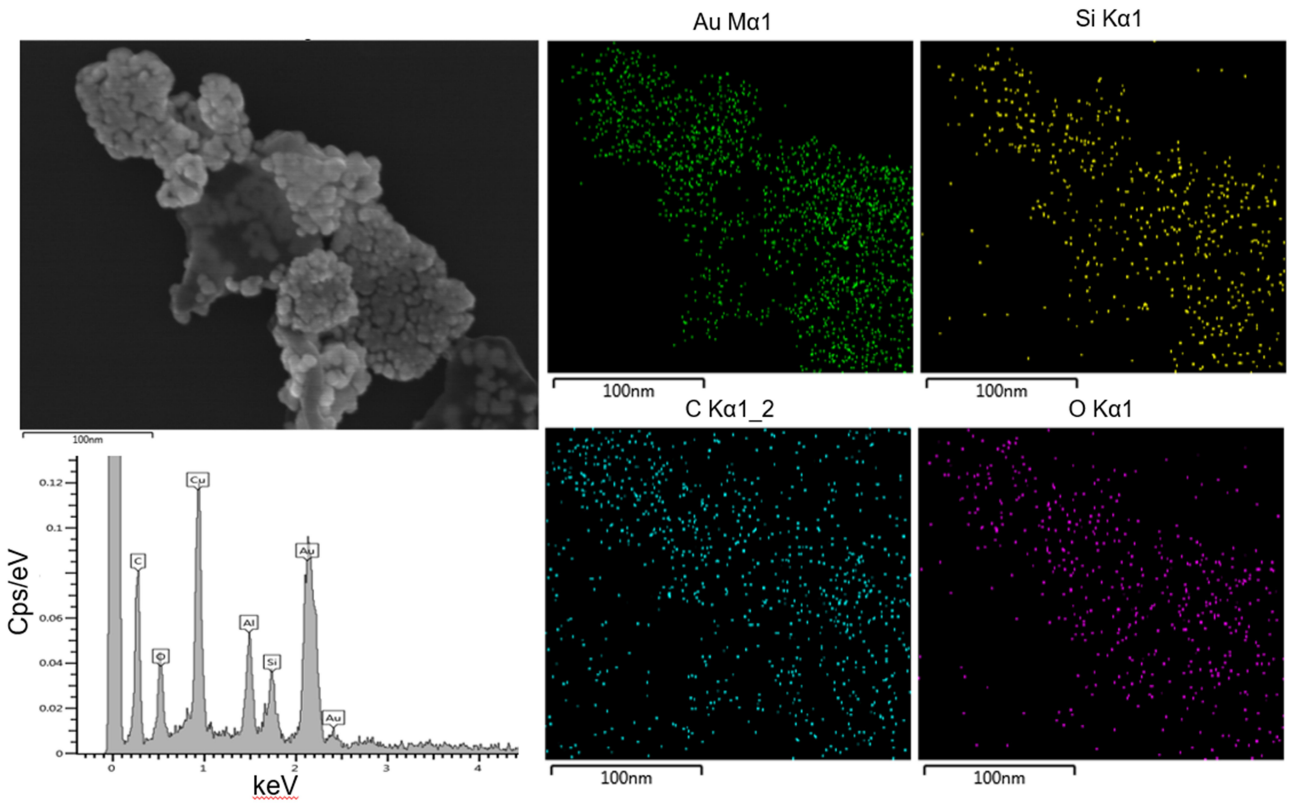

Figure 3 EDS map pattern and spectrum of the GO@SiO_2@AuNS hybrid.

concentration changed from 2 to 150 μg/mL. It showed a good linear relationship (Y = 12.61X, R^2 = 0.9999) between the concentration of GO@SiO_2@AuNS hybrid and the absorbance at 808 nm (Figure 5B). Hence, we concluded that the concentration of the hybrid has a positive effect on their light absorption intensity in the

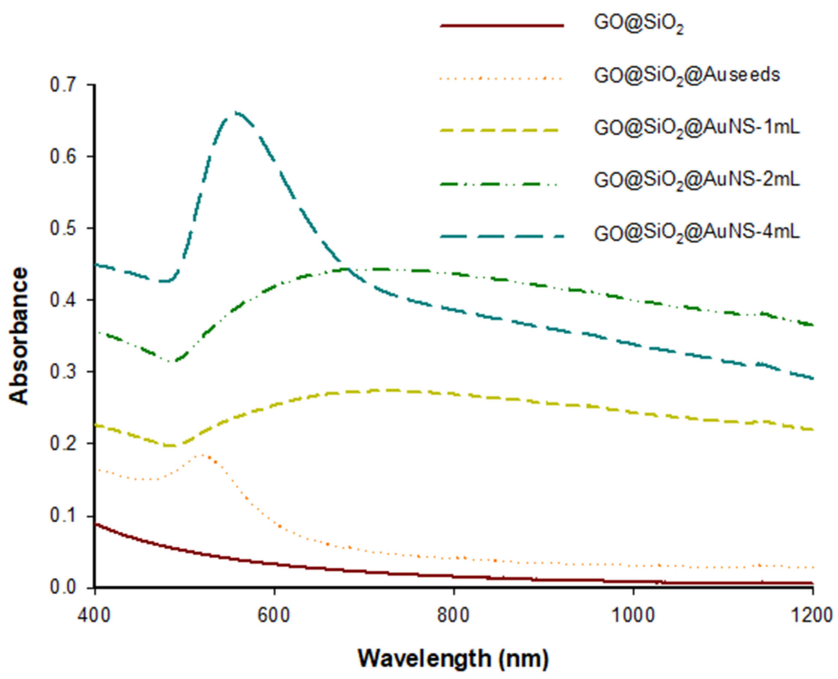

Figure 4 The absorption spectra of the synthesized nanomaterials.

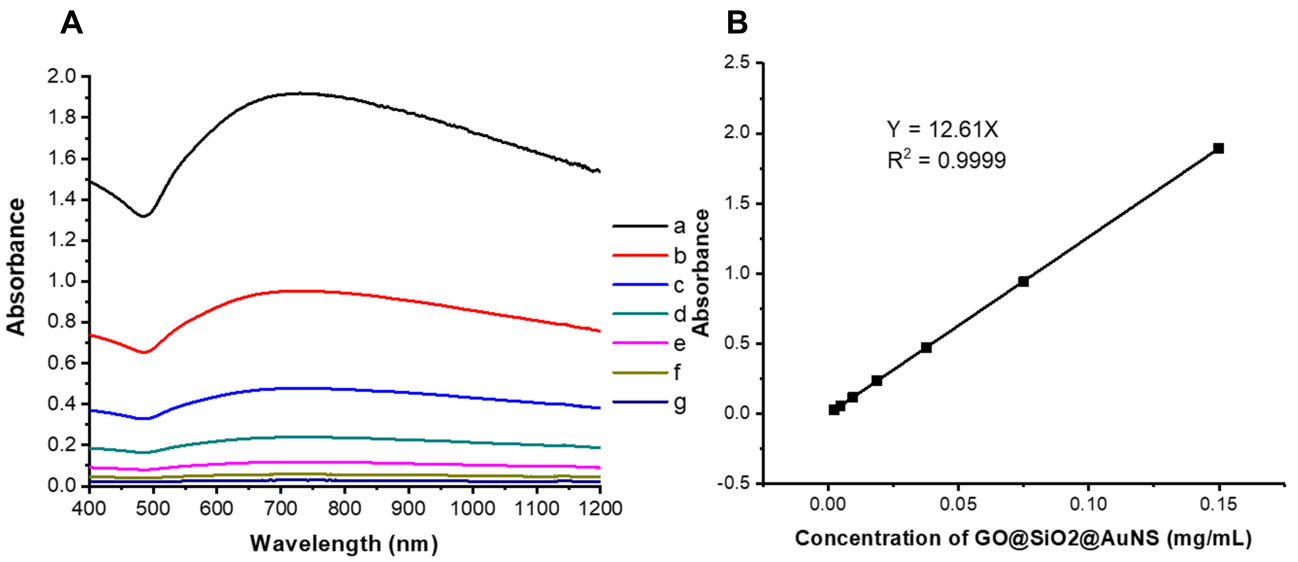

Figure 5 (**A**) The absorption spectra of GO@SiO_2@AuNS hybrid at different concentrations (a-g: 0.150, 0.075, 0.038, 0.019, 0.009, 0.005, to 0.002, mg/mL). (**B**) Linear relationship between the absorbance at 808 nm and the concentration of GO@SiO_2@AuNS hybrid.

near-infrared region, which can be strong even at a low concentration.

Photothermal Effect of GO@SiO_2@AuNS Hybrid

Motivated by the high NIR absorbance, the photothermal capability of GO@SiO_2@AuNS hybrid was further investigated by employing 808 NIR laser as an irradiation source. The temperature of the solutions was monitored for 20 min with the irradiation. As shown in Figure 6, the temperature of GO@SiO_2@AuNS hybrid showed a rapid increase upon the irradiation for a short period time of 10 min and reached a plateau after 20 min. Notably, a concentration-dependent temperature increase was demonstrated for GO@SiO_2@AuNS hybrid. The temperatures of GO@SiO_2@AuNS hybrid at 0.05, 0.10, to 0.15 mg/mL were enhanced by 9.1 °C, 11.7 °C, and 16.4 °C, respectively (Figure 6) with the irradiation for 20 min. In contrast, the temperature change of water and cell culture medium was less than 2 °C under the same condition. The results suggested that GO@SiO_2@AuNS hybrid has efficient photothermal conversion efficiency. The photothermal conversion efficiency of theGO@SiO_2@AuNS hybrid was calculated to be approximately 30%, which is higher than the gold nanorods (21.0%).[33]

Furthermore, the photothermal stability of GO@SiO_2@AuNS hybrid was evaluated. After the irradiation with 808 nm laser for 1 hour, the absorption spectra of GO@SiO_2@AuNS hybrid was recorded to compare with the original absorption spectrum. The results showed that NIR absorbance of GO@SiO_2@AuNS hybrid decreased by only 8.1% after 1-hour irradiation (Figure 7A), indicating the great photothermal stability of the GO@SiO_2@AuNS hybrid. The temperature changes of 0.15 mg/mL GO@SiO_2@AuNS hybrid solution in three laser on-off cycles were monitored to further prove the great photothermal stability. As shown in Figure 7B, after three cycles of laser exposure, the temperature of GO@SiO_2@AuNS hybrid solution decreased by only 2.5 °C compared with the first irradiation, implying the good photothermal stability as well.

Biocompatibility of the GO@SiO_2@AuNS Hybrid

To be used as an efficient photothermal agent for cancer therapy, the biocompatibility of GO@SiO_2@AuNS hybrid was evaluated by a standard MTT assay. We tested the biocompatibility of GO@SiO_2@AuNS hybrid in two cancer cell lines, including KM12C and SW620 cells. Various concentrations of GO@SiO_2@AuNS hybrid (0, 1, 5, 10, 25, 50, 75, and 100 μg/mL) were cultured with the cells at 37 °C for 24 h. As shown in Figure 8, the results demonstrated the concentration-dependent cytotoxicity of GO@SiO_2@AuNS hybrid for both cell lines. The cell viability decreased with the increased concentration of GO@SiO_2@AuNS hybrid. But importantly, the cell viability was still higher than 80% even with the highest concentration of 100

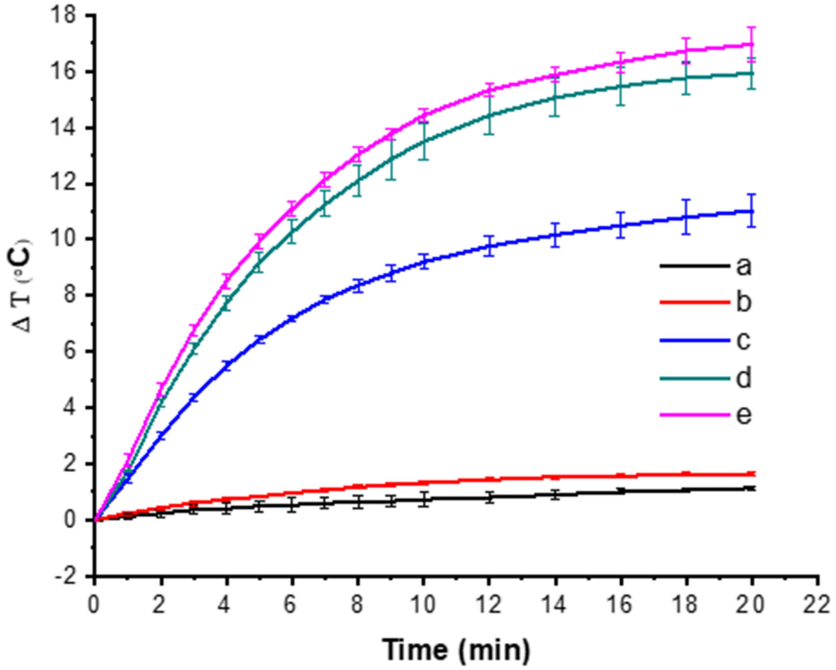

Figure 6 The heating curves of water (a), cell culture medium (b) and different concentrations of GO@SiO_2@AuNS hybrid (c to e: 0.05, 0.10, and 0.15 mg/mL).

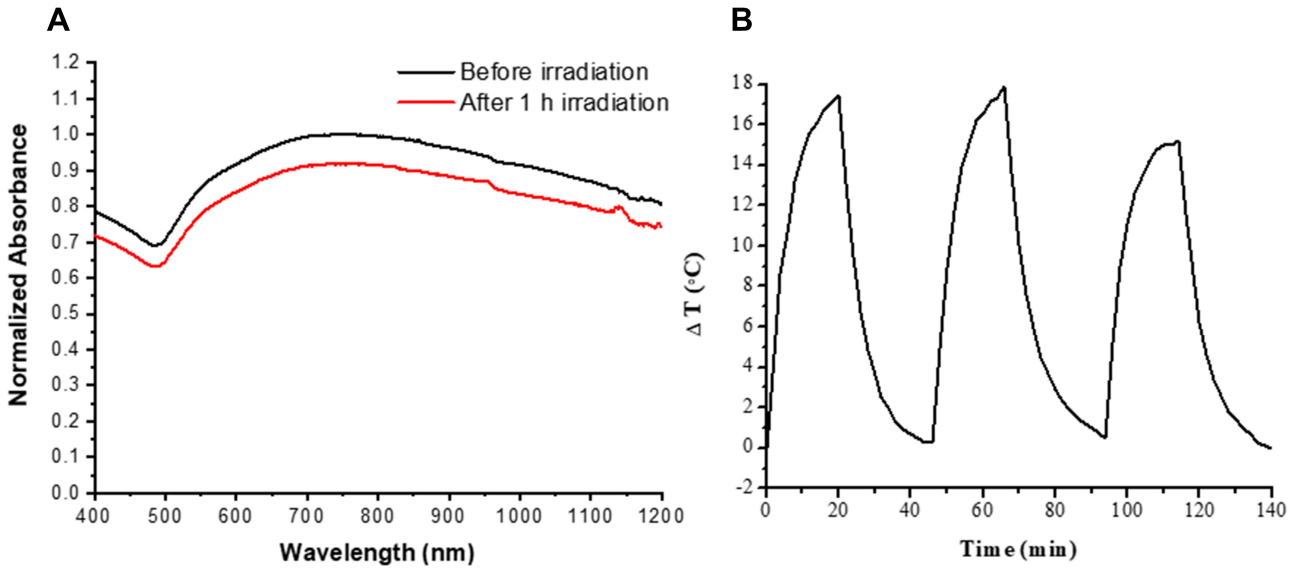

Figure 7 (**A**) Normalized absorption spectra of GO@SiO_2@AuNS hybrid before and after laser irradiation (0.3 W/cm^2 for 1 h). (**B**) Temperature changes of 0.15 mg/mL GO@SiO_2@AuNS hybrid under 808 nm laser irradiation for three cycle with the power density of 0.3 W/cm^2 (20 min of irradiation for each cycle).

μg/mL (Figure 8), indicating the good biocompatibility of the GO@SiO_2@AuNS hybrid.

In vitro Photothermal Therapy

Based on the superior photothermal properties and good biocompatibility, we explored the capacity of GO@SiO_2 @AuNS hybrid to destroy cancer cells under the NIR irradiation. The cell viability of KM12C cells under different treatments was assessed by MTT assay. As shown in Figure 9, either high concentration of GO@SiO_2@AuNS hybrid (100 μg/mL) or laser irradiation (0.3 W/cm^2 for 20 min) treatment alone showed negligible toxicity to cells. In contrast, the combination of GO@SiO_2 @AuNS hybrid and NIR laser irradiation significantly decreased cell viability. When the concentration of GO@SiO_2@AuNS hybrid was increased from 10, 50, to

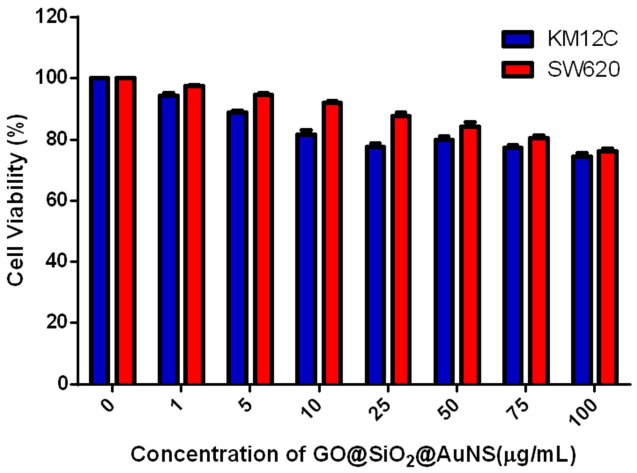

Figure 8 Relative cell viability after culturing with different concentrations of GO@SiO_2@AuNS hybrid varying from 0, 1, 5, 10, 25, 50, 75, and 100 μg/mL for 24 h at 37°C.

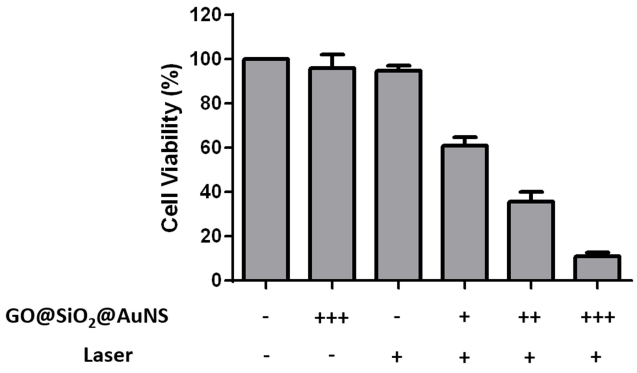

Figure 9 Relative cell viability after treatment of different concentrations of GO@SiO_2@AuNS hybrid in the presence or absence of NIR irradiation. - stands for no treatment. For the concentration of GO@SiO_2@AuNS hybrid, +, ++, and +++ represent the concentrations at 10, 50, and 100 μg/mL, respectively. For the laser irradiation, + represents 20 min NIR irradiation at 808 nm with 0.3 W/cm^2.

100 μg/mL with NIR laser irradiation, the cell viability was decreased to about 61%, 35%, and 10%, respectively.

Meanwhile, the in vitro photothermal therapy of GO@SiO_2@AuNS hybrid towards KM12C cells was further confirmed by Vybrant assay, which was used to distinguish apoptosis and necrosis through the green fluorescent YO-PRO-1 and red fluorescent propidium iodide (PI) staining, respectively. In Vybrant assay, YO-PRO-1 stains apoptotic cells, and PI stains necrotic cells. As shown in Figure 10, the fluorescence images demonstrated that only the cells treated with the combination of GO@SiO_2@AuNS hybrid and NIR laser irradiation could be stained with YO-PRO-1 and PI. The fluorescence intensities and the stained cell numbers were both enhanced when the concentration of GO@SiO_2@AuNS hybrid increased, which revealed that the effect of photothermal therapy is proportion to the concentration of GO@SiO_2@AuNS hybrid (Figure 10D–F). No fluorescence in green and red channels was observed with either the treatment of GO@SiO_2@AuNS hybrid or NIR laser irradiation alone. These results were consistent with the MTT result, confirming the photothermal ablation of the cells by GO@SiO_2@AuNS hybrid. Overall, the data suggested that GO@SiO_2@AuNS hybrid possessed an excellent photothermal therapeutic effect for KM12C cells under the low NIR laser irradiation.

Furthermore, to verify the cellular uptake of the prepared GO@SiO_2@AuNS hybrid in the tumor cell, a fluorescent dye, TAMRA, was doped into the mesoporous silica layer of the GO@SiO_2@AuNS hybrid. After the incubation of TAMRA doped GO@SiO_2@AuNS hybrid with KM12C cells, the cells were imaged using the confocal microscope to track the location of the hybrid. As shown in the Z-stack confocal fluorescence images (Figure 11), the TAMRA-labeled GO@SiO_2@AuNS hybrid mostly distributed in the cytoplasm of the KM12C cells, indicating the effective cellular uptake. Meanwhile, the successful carrying of TAMRA using the mesoporous silica layer suggested that the GO@SiO_2@AuNS hybrid has the potential to be used as a drug delivery system for chemotherapy as well. Coupled with the intrinsic photothermal therapy function, the GO@SiO_2@AuNS hybrid is promising for multi-modality therapy of cancer, which is under investigation in our lab.

Conclusions

In conclusion, we successfully designed and constructed a 2D GO@SiO_2@AuNS hybrid using a simple seed growth method. In this hybrid, the 2D GO was used as the template to form the 2D gold nanosheet. Interestingly, the novel GO@SiO_2@AuNS hybrid demonstrated strong NIR absorption due to the formation of the 2D gold nanosheet. Under the irradiation of 808 nm laser, the GO@SiO_2@AuNS hybrid showed great photothermal stability and significant photoablation of the cancer cells through the photothermal effect at a low laser dose (0.3 W/cm^2). Meanwhile, the GO@SiO_2@AuNS hybrid demonstrated excellent biocompatibility without laser irradiation. Together, this work suggests that the novel 2D GO@SiO_2@AuNS hybrid highlights the promise for cancer photothermal therapy, which may inspire further explorations of the 2D nanostructures for cancer theragnostic.

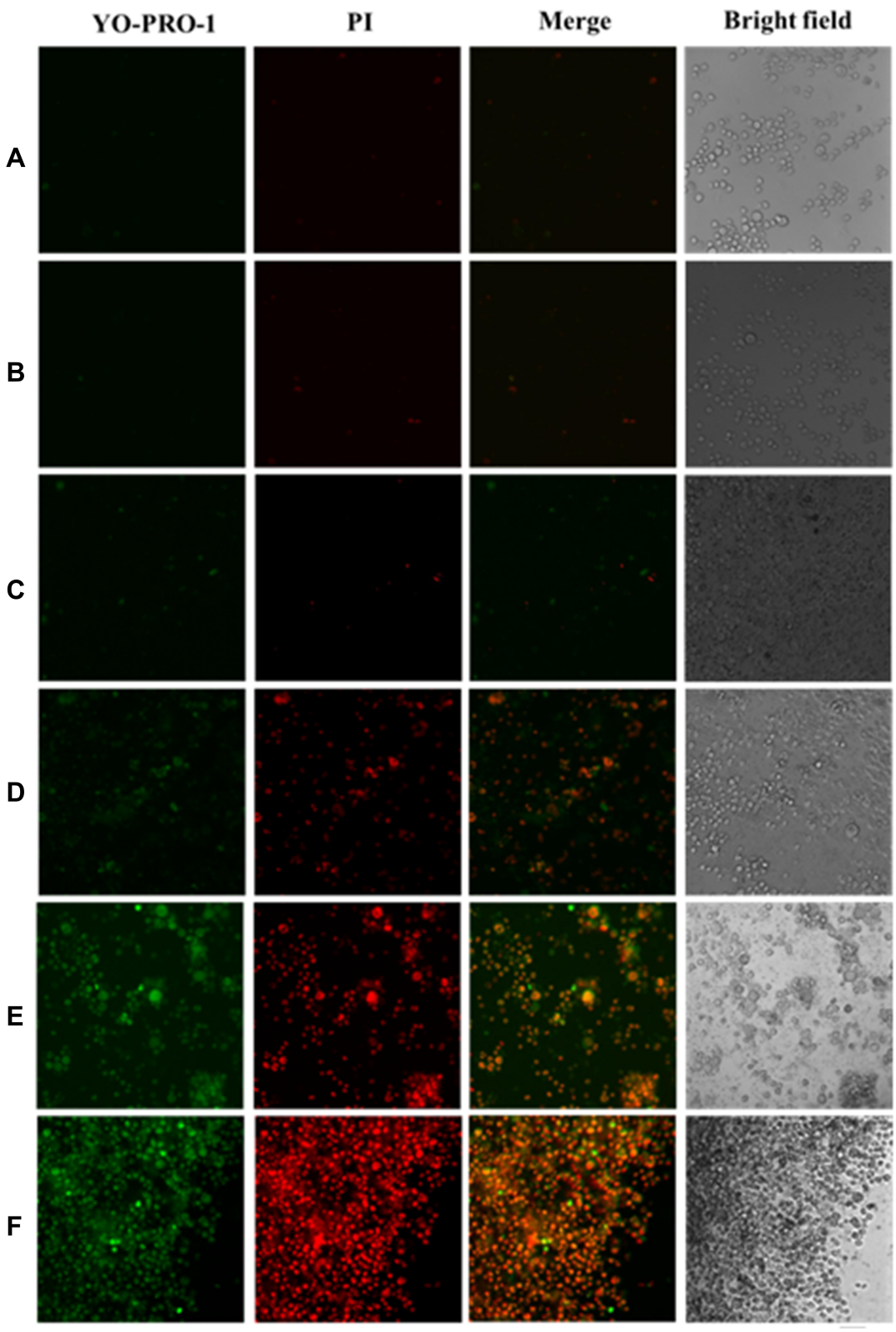

Figure 10 Fluorescence images of KM12C cells treated with different conditions: (**A**) without any treatment; (**B**) 20 min light exposure; (**C**) 100 μg/mL GO@SiO_2@AuNS hybrid; (**D**) 10 μg/mL GO@SiO_2@AuNS hybrid and 20 min light exposure; (**E**) 50 μg/mL GO@SiO_2@AuNS hybrid and 20 min light exposure; (**F**) 100 μg/mL GO@SiO_2 @AuNS hybrid and 20 min light exposure. The power intensity of light exposure was 0.3 W/cm^2. After the treatment, the cells were stained with Vybrant Apoptosis Assay. The green fluorescence from YO-PRO-1 showed the apoptotic cells, and the red fluorescence from PI showed the necrotic cells. Scale bar = 100 μm. A 20 X objective was used to capture the images.

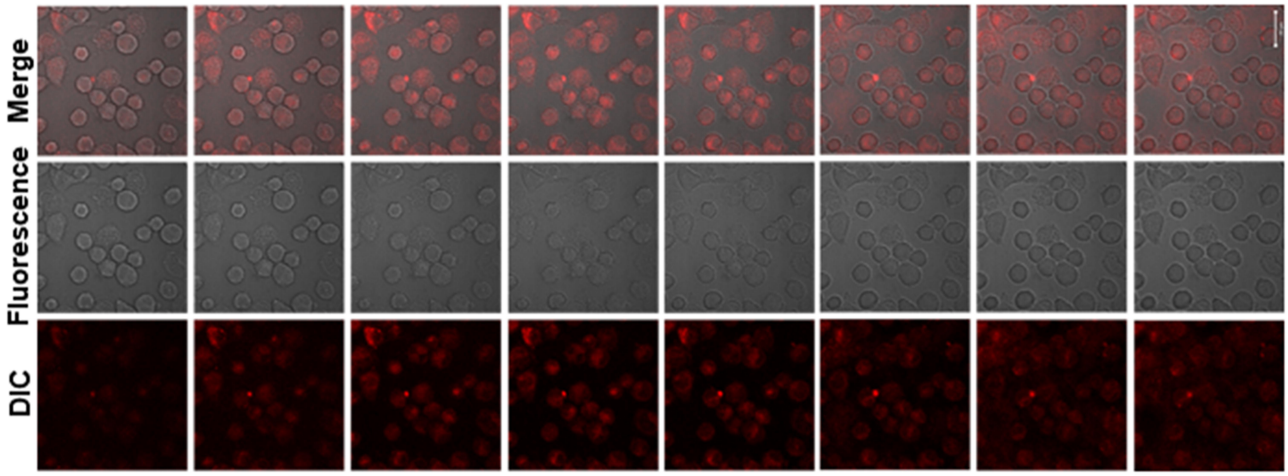

Figure 11 Confocal fluorescence images (Z-stack) of KM12C cells with the internalization of TAMRA doped GO@SiO_2@AuNS hybrid. KM12C cells were incubated with TAMRA doped GO@SiO_2@AuNS hybrid for 6 h at 37 °C before taking the images.

Abbreviations

NIR, near-infrared; GO@SiO_2@AuNS, graphene oxide-template gold nanoshell; PTT, photothermal therapy; MDR, multidrug resistance; NPs, nanoparticles; 2D, two-dimensional; GO, graphene oxide; TEOS, tetraethylorthosilicate; CTAB, hexadecyltrimethylammonium bromide; PVP, polyvinylpyrrolidone molecule; PI, propidium iodide.

Acknowledgments

We are grateful to the National Natural Science Foundation of China (21806186, 31741049), CSU Innovation-Driven funding (20180026040002), Huxiang high-level talent gathering project-innovative talents (2019RS1005) for the support of this work.

Disclosure

The authors report no conflicts of interest for this work.

References

1. Bray F, Ferlay J, Soerjomataram I, et al. Global cancer statistics 2018: GLOBOCAN estimates of incidence and mortality worldwide for 36 cancers in 185 countries. *CA Cancer J Clin*. 2018;68(6):394–424. doi:10.3322/caac.21492
2. Markham MJ, Wachter K, Agarwal N, et al. Clinical cancer advances 2020: annual report on progress against cancer from the American Society of Clinical Oncology. *J Clin Oncol*. 2020;38(10):1081. doi:10.1200/JCO.19.03141
3. Mirrahimi M, Abed Z, Beik J, et al. A thermo-responsive alginate nanogel platform co-loaded with gold nanoparticles and cisplatin for combined cancer chemo-photothermal therapy. *Pharmacol Res*. 2019;143:178–185. doi:10.1016/j.phrs.2019.01.005
4. Datta NR, Ordonez SG, Gaipl US, et al. Local hyperthermia combined with radiotherapy and-/or chemotherapy: recent advances and promises for the future. *Cancer Treat Rev*. 2015;41(9):742–753. doi:10.1016/j.ctrv.2015.05.009
5. Sparano JA, Gray RJ, Ravdin PM, et al. Clinical and genomic risk to guide the use of adjuvant therapy for breast cancer. *N Engl J Med*. 2019;380(25):2395–2405. doi:10.1056/NEJMoa1904819
6. Cheng L, Wang C, Feng L, Yang K, Liu Z. Functional nanomaterials for phototherapies of cancer. *Chem Rev*. 2014;114(21):10869–10939. doi:10.1021/cr400532z
7. Kong G. Review Hyperthermia and liposomes. *Int J Hyperther*. 1999;15(5):345–370. doi:10.1080/026567399285558
8. de Melo-diogo D, Pais-Silva C, Dias DR, Moreira AF, Correia IJ. Strategies to improve cancer photothermal therapy mediated by nanomaterials. *Adv Healthc Mater*. 2017;6(10):1700073. doi:10.1002/adhm.201700073
9. Gao G, Jiang Y-W, Guo Y, et al. Enzyme-mediated tumor starvation and phototherapy enhance mild-temperature photothermal therapy. *Adv Funct Mater*. 2020;30(16):1909391. doi:10.1002/adfm.201909391
10. Zhu YX, Jia HR, Gao G, et al. Mitochondria-acting nanomicelles for destruction of cancer cells via excessive mitophagy/autophagy-driven lethal energy depletion and phototherapy. *Biomaterials*. 2020;232:119668. doi:10.1016/j.biomaterials.2019.119668
11. Gao G, Jiang Y-W, Sun W, et al. Molecular targeting-mediated mild-temperature photothermal therapy with a smart albumin-based nanodrug. *Small*. 2019;15(33):1900501. doi:10.1002/smll.201900501
12. Zhang S, Guo W, Wei J, et al. Terrylenediimide-based intrinsic theranostic nanomedicines with high photothermal conversion efficiency for photoacoustic imaging-guided cancer therapy. *ACS Nano*. 2017;11(4):3797–3805. doi:10.1021/acsnano.6b08720
13. Ge J, Jia Q, Liu W, et al. Red-emissive carbon dots for fluorescent, photoacoustic, and thermal theranostics in living mice. *Adv Mater*. 2015;27(28):4169–4177. doi:10.1002/adma.201500323
14. Wang X, Wang C, Cheng L, Lee ST, Liu Z. Noble metal coated single-walled carbon nanotubes for applications in surface enhanced Raman scattering imaging and photothermal therapy. *J Am Chem Soc*. 2012;134(17):7414–7422. doi:10.1021/ja300140c
15. Ghaznavi H, Hosseini-Nami S, Kamrava SK, et al. Folic acid conjugated PEG coated gold-iron oxide core-shell nanocomplex as a potential agent for targeted photothermal therapy of cancer. *Artif Cells Nanomed Biotechnol*. 2018;46(8):1594–1604. doi:10.1080/21691401.2017.1384384
16. Johnsen KB, Bak M, Melander F, et al. Modulating the antibody density changes the uptake and transport at the blood-brain barrier of both transferrin receptor-targeted gold nanoparticles and liposomal cargo. *J Control Release*. 2019;295:237–249. doi:10.1016/j.jconrel.2019.01.005

17. Lee HE, Ahn HY, Mun J, et al. Amino-acid- and peptide-directed synthesis of chiral plasmonic gold nanoparticles. *Nature*. 2018;556 (7701):360–365. doi:10.1038/s41586-018-0034-1
18. Samadian H, Hosseini-Nami S, Kamrava SK, Ghaznavi H, Shakeri-Zadeh A. Folate-conjugated gold nanoparticle as a new nanoplatform for targeted cancer therapy. *J Cancer Res Clin Oncol*. 2016;142 (11):2217–2229. doi:10.1007/s00432-016-2179-3
19. Her S, Jaffray DA, Allen C. Gold nanoparticles for applications in cancer radiotherapy: mechanisms and recent advancements. *Adv Drug Deliv Rev*. 2017;109:84–101. doi:10.1016/j.addr.2015.12.012
20. Chen YS, Zhao Y, Yoon SJ, Gambhir SS, Emelianov S. Miniature gold nanorods for photoacoustic molecular imaging in the second near-infrared optical window. *Nat Nanotechnol*. 2019;14(5):465–472. doi:10.1038/s41565-019-0392-3
21. Zhang D, Qin X, Wu T, et al. Extracellular vesicles based self-grown gold nanopopcorn for combinatorial chemo-photothermal therapy. *Biomaterials*. 2019;197:220–228. doi:10.1016/j.biomaterials.2019.01.024
22. Liu Y, Yang M, Zhang J, et al. Human induced pluripotent stem cells for tumor targeted delivery of gold nanorods and enhanced photothermal therapy. *ACS Nano*. 2016;10(2):2375–2385. doi:10.1021/acsnano.5b07172
23. Chen H, Zhang X, Dai S, et al. Multifunctional gold nanostar conjugates for tumor imaging and combined photothermal and chemo-therapy. *Theranostics*. 2013;3(9):633–649. doi:10.7150/thno.6630
24. Topete A, Alatorre-Meda M, Iglesias P, et al. Fluorescent drug-loaded, polymeric-based, branched gold nanoshells for localized multimodal therapy and imaging of tumoral cells. *ACS Nano*. 2014;8 (3):2725–2738. doi:10.1021/nn406425h
25. Tang W, Dong Z, Zhang R, et al. Multifunctional two-dimensional core-shell MXene@Gold nanocomposites for enhanced photo-radio combined therapy in the second biological window. *ACS Nano*. 2019;13(1):284–294. doi:10.1021/acsnano.8b05982
26. Yan H, Tao X, Yang Z, et al. Effects of the oxidation degree of graphene oxide on the adsorption of methylene blue. *J Hazard Mater*. 2014;268:191–198. doi:10.1016/j.jhazmat.2014.01.015
27. Zhang L, Xia J, Zhao Q, Liu L, Zhang Z. Functional graphene oxide as a nanocarrier for controlled loading and targeted delivery of mixed anticancer drugs. *Small*. 2010;6(4):537–544. doi:10.1002/smll.200901680
28. Yang X, Wang Y, Huang X, et al. Multi-functionalized graphene oxide based anticancer drug-carrier with dual-targeting function and pH-sensitivity. *J Mater Chem*. 2011;21(10):3448–3454. doi:10.1039/C0JM02494E
29. Gao S, Zhang L, Wang G, et al. Hybrid graphene/Au activatable theranostic agent for multimodalities imaging guided enhanced photothermal therapy. *Biomaterials*. 2016;79:36–45. doi:10.1016/j.biomaterials.2015.11.041
30. Zeng Y, Yang Z, Li H, et al. Multifunctional nanographene oxide for targeted gene-mediated thermochemotherapy of drug-resistant tumour. *Sci Rep*. 2017;7:43506. doi:10.1038/srep43506
31. Liu X, Wu X, Xing Y, et al. Reduced graphene oxide/mesoporous silica nanocarriers for pH-triggered drug release and photothermal therapy. *ACS Appl Biol Mater*. 2020;3(5):2577–2587. doi:10.1021/acsabm.9b01108
32. Chen J, Li X, Wu X, et al. Au-Silica nanowire nanohybrid as a hyperthermia agent for photothermal therapy in the near-infrared region. *Langmuir*. 2014;30(31):9514–9523. doi:10.1021/la5020434
33. Li S, Deng Q, Li X, et al. Bis-diketopyrrolopyrrole conjugated polymer nanoparticles as photothermic nanoagonist for specific and synergistic glioblastoma therapy. *Biomaterials*. 2019;216:119252. doi:10.1016/j.biomaterials.2019.119252